Ultrafast self-action of surface-plasmon polaritons at an air/metal interface

Alexandre Baron,[1,2] Thang B. Hoang,[1,3] Chao Fang,[1,2] Maiken H. Mikkelsen,[1,2,3] and David R. Smith[1,2,3]

[1]*Center for Metamaterials and Integrated Plasmonics, Duke University, Durham, North Carolina 27708, USA*

[2]*Department of Electrical and Computer Engineering, Duke University, Durham, North Carolina 27708, USA*

[3]*Department of Physics, Duke University, Durham, North Carolina 27708, USA*

We investigate both theoretically and experimentally the nonlinear propagation of surface-plasmon polaritons (SPP) on a single air/metal interface. Inspired by nonlinear dielectric waveguide theory, we analytically derive a model that describes the nonlinear propagation of SPPs, thus bridging the description of plasmonic and dielectric waveguides. The model, the numerical simulations, and the experiments, which are carried out in the 100 fs regime, reveal that the SPP undergoes strong ultrafast self-action which manifests itself through self-induced absorption. Our observations are consistent with a large, bulk, third-order nonlinear susceptibility ($\chi^{(3)}$) of gold and provide a self-consistent theory of self-action of SPPs at an air/metal interface. Experimentally, we find $\mathrm{Im}\{\chi^{-(3)}\} \sim 3 \times 10^{-16}\,\mathrm{m^2/V^2}$. These findings have important implications in the nonlinear physics of plasmonics and metamaterials as they provide evidence that nonlinear absorption has a significant effect on the propagation of SPPs excited by intense optical pulses. This self-action is also expected to affect the anomalous absorption of light near subwavelength structures as well as the strength of desirable nonlinear processes such as third-harmonic generation and four-wave mixing, which will inevitably compete with nonlinear absorption.

I. INTRODUCTION

A surface-plasmon polariton (SPP) is a coupled oscillation of electromagnetic radiation and charge density at an interface between a metal and a dielectric [1]. These waves are tightly confined to the metallic surface over subwavelength dimensions and may propagate parallel to the surface for several tens or hundreds of microns before their energy is dissipated by resistive losses. The single metal/dielectric interface thus acts as a single-mode waveguide for these surface waves and—in the case where the dielectric is a vacuum—the waveguide has an effective index given by

$$n_{\mathrm{eff}} = \left(\frac{\varepsilon_{\mathrm{m}}}{1 + \varepsilon_{\mathrm{m}}} \right)^{1/2}, \qquad (1)$$

where ε_{m} is the dielectric constant of the metal. Because of their ability to concentrate light in subwavelength volumes, SPPs are of particular interest in nonlinear optics, where enhancing power densities lowers the nonlinear thresholds [2,3]. Artificially structured metamaterials incorporating plasmonic components offer a promising route to enhancing nonlinear processes [4–6]; however, many open questions remain to fully understand the physics of nonlinear phenomena in conductors that provide the plasmonic response. In most of the nonlinear plasmonic configurations investigated thus far, the dielectric component has been assumed to provide the dominant nonlinear system response [5–12]. However, metals are known to have relatively large nonlinear susceptibilities, making SPPs intrinsically nonlinear excitations [13–17]. The nonlinear response of metals is complex, with different mechanisms that depend on the time scale over which the response is probed. For instance, the 100 fs regime probes the smearing of the Fermi-Dirac distribution due to photoexcited hot electrons, and the subsequent heat transferred to the conduction electrons through thermalization. Moving into the picosecond regime, the probed nonlinearity consists of heat dissipation into the metal lattice due to thermalization of

the conduction electrons. Both regimes produce third-order nonlinear susceptibilities $\chi^{(3)}$ that span several orders of magnitude [16]. Aside from these three mechanisms, previous experiments have also indicated that interband transitions and two-photon absorption produce a very large, ultrafast, effective third-order susceptibility [15,18]. Furthermore, using thermoreflectance, Lozan *et al.* recently probed the heat dissipated near a subwavelength slit under high-intensity pumping [19]. Using a pump laser at 800 nm with a pulse duration of 180 fs, their measurements show that heat dissipation exhibits a constant absorption plateau. While this result is intriguing and may very well have new and profound implications on the underlying physics of surface-plasmon propagation, this observation combined with the wide variety of nonlinear phenomena occurring in gold shows how little is known regarding the propagation of intense SPPs.

Inspired by the formalism used for nonlinear dielectric waveguides, we develop an analytical description of the simplest plasmonic waveguide: the single air/metal interface (see Fig. 1) that provides a closed-form expression for the power density of the SPP undergoing self-induced absorption; we then relate the effective nonlinear absorption coefficient β_{eff} to the third-order nonlinear susceptibility of gold (Sec. II). We investigate experimentally the propagation of intense SPPs along a single air/gold interface for varying waveguide lengths and show that our formalism provides an accurate fit to our experimental data (Sec. III). Here we investigate the ultrafast self-action of SPPs that solely probes the gold nonlinearity and reveals the effect it has on SPP propagation. This experimental test enables us to retrieve a value for the imaginary part of $\chi^{(3)}$. Comparisons among the analytical model, the experiment, and full-wave numerical simulations are consistent with a strong self-induced absorption of the SPP due to the nonlinearity of the metal. Finally, we relate $\mathrm{Im}\{\chi^{(3)}\}$ to excess electrons generated by interband absorption based solely on the fundamental linear properties of gold (Sec. IV).
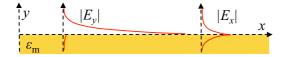
FIG. 1. (Color online) Sketch of the single-interface SPP waveguide consisting of a semi-infinite slab of metal adjacent to air. The modulus of the longitudinal (E_x) and transverse field (E_y) profiles are shown.

II. MODEL OF SELF-ACTION OF SURFACE-PLASMON POLARITONS

The propagation of single-mode dielectric waveguides at optical frequencies is well described by the nonlinear Schrödinger equation (NLSE), i.e., the propagation equation applied to a perturbed fundamental mode and where the polarization is expanded into a power series of the electric field [20]. We apply the same type of formalism here to the single-interface plasmonic waveguide. Though nonlinear plasmonic and dielectric waveguides are analogous to some extent, there are notable differences. For instance, in the single-interface plasmonic waveguide sketched in Fig. 1, the longitudinal component of the electric field is dominant in the metal region such that it constitutes the major contributor to the nonlinear response [21]. In addition, the optical index associated with metals usually has a very large imaginary part compared with that of dielectrics, whose indices are predominantly real. As a consequence, both the real and the imaginary parts of the metal nonlinear susceptibility $\chi^{(3)}$ act on the phase as well as on the amplitude of the field, whereas for dielectric waveguides the real part drives the phase modulation and the imaginary part drives the modulation of amplitude [22,23]. Another very important property of the nonlinear SPP is that self-action mostly takes the form of self-induced absorption rather than self-phase modulation, since the intensity-dependent phase shift produced by $\chi^{(3)}$ is small compared to the intensity-dependent absorption [13]. If dielectric and plasmonic nonlinear waveguides are analogous in the sense of transported power, then by considering the power per unit length $S(x)$, defined as the power flow along the x direction of the time-averaged Poynting vector $S(x) = 1/2\mathrm{Re} \int (\mathbf{E} \times \mathbf{H}^*) \cdot \hat{\mathbf{x}} dy$, the NLSE should simplify to a first-order nonlinear differential equation [22,23]

$$\frac{\partial S}{\partial x} = -\alpha_{\mathrm{eff}} S - \beta_{\mathrm{eff}} S^2, \tag{2}$$

where $\alpha_{\mathrm{eff}} = 4\pi \, \mathrm{Im}(n_{\mathrm{eff}})/\lambda$ is the effective linear absorption coefficient of the SPP waveguide and x is the propagation direction.

We seek to establish an analytic relation between β_{eff} and $\chi^{(3)}$ for the single air/metal interface. Here we provide the important steps and approximations that lead to deriving a simplified version of this relation that captures the essential physics, and refer the interested reader to our Supplemental Material for a comprehensive derivation [24]. We consider the third-order nonlinear polarization $\mathbf{P^{(3)}}$ to be a small perturbation and start by writing the NLSE: $(\nabla^2 + k_0^2 n_{\mathrm{eff}}^2)\mathbf{E} = \mu_0 \omega^2 \mathbf{P^{(3)}}$, where $k_0 = \omega/c = 2\pi/\lambda$ is the free-space wave vector. The SPP field is the unique solution to the unperturbed propagation equation, i.e., when the right-hand term in the NLSE is zero, and is given by

$$\mathbf{E}_{\mathrm{SPP}} = E_0 e^{ik_0 n_{\mathrm{eff}} x} \begin{cases} e^{ik_0 n_\perp^{\mathrm{d}} y}(-n_\perp^{\mathrm{d}} \hat{\mathbf{x}} + n_{\mathrm{eff}} \hat{\mathbf{y}}) & \text{for } y > 0 \\ e^{-ik_0 n_\perp^{\mathrm{m}} y} \left[\frac{n_\perp^{\mathrm{m}}}{\varepsilon_{\mathrm{m}}} \hat{\mathbf{x}} + \frac{n_{\mathrm{eff}}}{\varepsilon_{\mathrm{m}}} \hat{\mathbf{y}} \right] & \text{for } y < 0, \end{cases} \tag{3}$$

where $n_\perp^{\mathrm{d}} = (1 - n_{\mathrm{eff}}^2)^{1/2}$ and $n_\perp^{\mathrm{m}} = (\varepsilon_{\mathrm{m}} - n_{\mathrm{eff}}^2)^{1/2}$ [25]. By considering the nonlinear polarization to be a small perturbation to the linear polarization and assuming the SPP to maintain its state of polarization, we may consider $\xi \, \mathbf{E}_{\mathrm{SPP}}$ to be a solution to the NLSE, where ξ is a scalar. Treating the nonlinear polarization as a perturbation means that ξ should remain nearly constant over one wavelength ($\delta|\xi| \ll \lambda k_0 |\mathrm{Im}\{n_{\mathrm{eff}}\}\|\xi|$ and $\delta\phi_\xi = \delta[\arg(\xi)] \ll \lambda k_0 |\mathrm{Re}\{n_{\mathrm{eff}}\}|$). Next, we make the slowly varying envelope approximation, use the unperturbed propagation equation, and apply the dot product with the complex conjugate of $\mathbf{E}_{\mathrm{SPP}}$, such that the NLSE reduces to

$$\frac{\partial \xi}{\partial x} = -\frac{i\mu_0 \omega^2}{2k_0 n_{\mathrm{eff}}} \frac{\int_{y<0} \mathbf{P^{(3)}} \mathbf{E}_{\mathrm{SPP}}^* dy}{\int_{-\infty}^{+\infty} \|\mathbf{E}_{\mathrm{SPP}}\|^2 dy}. \tag{4}$$

The integral in the numerator is carried out only for $y < 0$, as only the metal nonlinearity is considered here, where we can make the approximation that the fields involved in the nonlinear polarization in the gold are mostly longitudinal [21]. Overall, the power of the SPP is mostly carried by the transverse field in the dielectric. For self-action, the nonlinear polarization is $\mathbf{P^{(3)}} = 3/4\varepsilon_0 \chi^{(3)} |\xi|^2 \xi \|\mathbf{E}_{\mathrm{SPP}}\|^2 \mathbf{E}_{\mathrm{SPP}}$. Introducing this nonlinear polarization into Eq. (4), we evaluate the integrals and get the following differential equation [24]:

$$\frac{\partial \xi}{\partial x} = i \frac{3}{16} \frac{k_0}{|n_{\mathrm{eff}}|^2} \frac{\mathrm{Im}\, n_\perp^{\mathrm{d}}}{\mathrm{Im}\, n_\perp^{\mathrm{m}}} \left| \frac{n_\perp^{\mathrm{m}}}{\varepsilon_{\mathrm{m}}} \right|^4 \left[\mathrm{Re}\left\{ \frac{\chi^{(3)}}{n_{\mathrm{eff}}} \right\} \right.$$
$$\left. + i\, \mathrm{Im}\left\{ \frac{\chi^{(3)}}{n_{\mathrm{eff}}} \right\} \right] E_0^2 |\xi|^2 \xi. \tag{5}$$

The following relation holds for ξ

$$\frac{\partial \xi}{\partial x} = \left(\frac{1}{|\xi|} \frac{\partial |\xi|}{\partial x} + i \frac{\partial \phi_\xi}{\partial x} \right) \xi. \tag{6}$$

By comparing it with Eq. (5), we see that $\mathrm{Re}\{\chi^{(3)}/n_{\mathrm{eff}}\}$ is the nonlinear term that acts on the phase of the perturbed field, whereas $\mathrm{Im}\{\chi^{(3)}/n_{\mathrm{eff}}\}$ is the nonlinear term that acts on the amplitude of the perturbed field. We use the relation linking S to $|\xi|^2$ given by Eq. (10) in Ref. [24] and identify Eq. (6) with Eq. (5) to write the following differential equation:

$$\frac{1}{|\xi|} \frac{\partial |\xi|}{\partial x} = -\frac{3}{4} \frac{k_0^2 Z_0}{\mathrm{Re}\, n_{\mathrm{eff}} |n_{\mathrm{eff}}|^2} \left| \frac{n_\perp^{\mathrm{m}}}{\varepsilon_{\mathrm{m}}} \right|^4 \frac{(\mathrm{Im}\, n_\perp^{\mathrm{d}})^2}{\mathrm{Im}\, n_\perp^{\mathrm{m}}} \mathrm{Im}\left\{ \frac{\chi^{(3)}}{n_{\mathrm{eff}}} \right\} S, \tag{7}$$

where Z_0 is the free-space impedance. Finally, by using the identity $1/|\xi| \times \partial|\xi|/\partial x = 1/(2S) \times \partial S/\partial x$ with Eq. (7) and identifying with Eq. (2), we arrive at the following relation for the nonlinear absorption coefficient:

$$\beta_{\mathrm{eff}} = \frac{3}{2} \frac{k_0^2 Z_0}{\mathrm{Re}\, n_{\mathrm{eff}} |n_{\mathrm{eff}}|^2} \left| \frac{n_\perp^{\mathrm{m}}}{\varepsilon_{\mathrm{m}}} \right|^4 \frac{(\mathrm{Im}\, n_\perp^{\mathrm{d}})^2}{\mathrm{Im}\, n_\perp^{\mathrm{m}}} \mathrm{Im}\left\{ \frac{\chi^{(3)}}{n_{\mathrm{eff}}} \right\}. \tag{8}$$

We see here that in contrast to nonlinear dielectric waveguides [22,23], β_{eff} is related to the imaginary part of the ratio between the third-order susceptibility and the effective

index. However, since $n_{\mathrm{eff}} \sim \mathrm{Re}(n_{\mathrm{eff}})$, Eq. (8) relates β_{eff} and $\mathrm{Im}\{\chi^{(3)}\}$.

In the case considered here, Eq. (2) can straightforwardly be integrated. The solution describes the evolution of the SPP power per unit length as

$$S(x) = \frac{S_{\text{B-L}}(x) S_{\text{sat}}(x)}{S_{\text{B-L}}(x) + S_{\text{sat}}(x)}, \tag{9}$$

where $S_{\text{B-L}}(x) = S_0 e^{-\alpha_{\mathrm{eff}} x}$ and $S_{\text{sat}}(x) = \alpha_{\mathrm{eff}} e^{-\alpha_{\mathrm{eff}} x}/[\beta_{\mathrm{eff}}(1 - e^{-\alpha_{\mathrm{eff}} x})]$. Interestingly, $S(x)$ exhibits a saturable behavior, as it evolves linearly following the classical Beer-Lambert law given by $S_{\text{B-L}}(x)$ in the limit of small $S_0(\ll \alpha_{\mathrm{eff}}/\beta_{\mathrm{eff}})$ and saturates to the constant value $S_{\text{sat}}(x)$ in the limit of large $S_0(\gg \alpha_{\mathrm{eff}}/\beta_{\mathrm{eff}})$. The functional dependence of S with x is related to that of $|\xi(x)|$, which is given by

$$|\xi(x)| = [1 + \beta_{\mathrm{eff}} S_0 (1 - e^{-\alpha_{\mathrm{eff}} x})/\alpha_{\mathrm{eff}}]^{-1/2}. \tag{10}$$

We can produce a similar identification between Eq. (5) and Eq. (6) as was done for $|\xi|$, to write the following differential equation for ϕ_ξ:

$$\frac{\partial \phi_\xi}{\partial x} = k_0 n_2^{\mathrm{eff}} S, \tag{11}$$

where n_2^{eff} is the effective intensity-dependent index for the SPP. This coefficient produces self-phase modulation of the SPP and is equal to

$$n_2^{\mathrm{eff}} = \frac{3}{4} \frac{k_0 Z_0}{\mathrm{Re}\, n_{\mathrm{eff}} |n_{\mathrm{eff}}|^2} \left| \frac{n_\perp^{\mathrm{m}}}{\varepsilon_{\mathrm{m}}} \right|^4 \frac{(\mathrm{Im}\, n_\perp^{\mathrm{d}})^2}{\mathrm{Im}\, n_\perp^{\mathrm{m}}} \mathrm{Re}\left\{ \frac{\chi^{(3)}}{n_{\mathrm{eff}}} \right\}. \tag{12}$$

Equation (11) integrates into this formula relating ϕ_ξ to $|\xi|$:

$$\phi_\xi = -\frac{\mathrm{Re}\{\chi^{(3)}\}}{\mathrm{Im}\{\chi^{(3)}\}} \ln|\xi|, \tag{13}$$

where we have used the approximation $n_{\mathrm{eff}} \sim \mathrm{Re}(n_{\mathrm{eff}})$ again. To compare the nonlinear phase shift ϕ_ξ with the nonlinear power transmission $|\xi|^2$, we assume that both real and imaginary parts of $\chi^{(3)}$ are almost equal in Eq. (13). Figure 2 compares $|\xi|^2$ with ϕ_ξ, as a function of the dimensionless parameter $\kappa = \beta_{\mathrm{eff}} S_0 (1 - e^{-\alpha_{\mathrm{eff}} x})/\alpha_{\mathrm{eff}}$, which governs the strength of the nonlinear response ($|\xi|^2 = 1/[1 + \kappa]$ and $\phi_\xi \sim 0.5 \ln[1 + \kappa]$). We see that for $\kappa \in [0,1]$, transmission is reduced by half compared to the linear regime, while
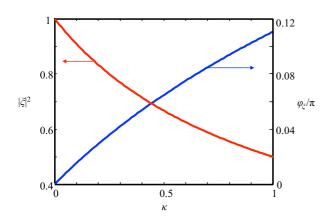
FIG. 2. (Color online) Comparison between nonlinear transmission $|\xi|^2$ (in red) and nonlinear phase shift ϕ_ξ (in blue) as a function of the dimensionless nonlinear strength parameter κ.

the accumulated nonlinear phase shift is very small. This confirms that self-action mostly takes the form of self-induced absorption rather than self-phase modulation.

III. EXPERIMENTAL EVIDENCE OF ULTRAFAST SELF-ACTION

Next, we test Eq. (9) experimentally by exciting SPPs along an air/gold interface with a pulsed Ti:sapphire laser operating at $\lambda = 800$ nm. The pulses have a FWHM duration $\tau \sim 100$ fs and a repetition rate $\nu_{\mathrm{rep}} = 80$ MHz. The waveguides consist of a 265-nm-thick gold film, which can be considered as a semi-infinite substrate (~ 22 skin depths), on top of which asymmetric grating couplers and decouplers are fabricated by using electron beam lithography with subsequent liftoff [24]. Each device consists of a coupler and decoupler with a separation distance d. Twenty-five devices are built with varying lengths d. The typical layout of a single waveguide is shown in Fig. 3(b). The coupler is designed to achieve high energy coupling from a beam incident normal to the interface. The norm of the simulated Poynting vector of the fields scattered by the designed coupler is shown in Fig. 3(a) [24]. The decoupler is a flipped coupler. The asymmetric grating design is essential as it ensures that the coupling and decoupling efficiencies are almost equal due to time-reversal symmetry. All the light coming from the sample is imaged on a CCD camera [see Fig. 3(c)]. The design of the gratings and details of the method used for the linear characterization of the waveguides can be found in [24,26]. This analysis enables the retrieval of the coupling/decoupling efficiency $\eta \sim 32\%$ as well as the linear absorption coefficient of the SPP $\alpha_{\mathrm{eff}} = 33$ mm^{-1} [see Fig. 3(d) for the transmission data T].

After calibrating and checking that both our optics and detection scheme are linear as the input laser power is
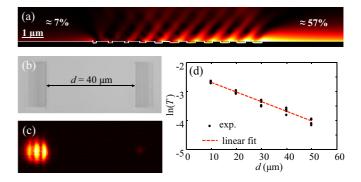
FIG. 3. (Color online) Design, fabrication, and linear characterization of the SPP waveguides. (a) Computed norm of the Poynting vector near the optimized coupler. 57% of the energy of a normally incident plane wave impinging on the width of the grating cross section is coupled to an SPP traveling toward the right-hand side and only 7% of the incoming energy is coupled to the opposite side. (b) White light image of a representative SPP waveguide fabricated consisting in a coupler (left) and a decoupler (right). (c) CCD image of the sample when the laser spot is shone on the coupler. (d) $\ln(T)$ vs d. The dots are the experimental data which was gathered by characterizing 25 devices in the 100 μW regime. The slope provides a measurement of α_{eff} and the y intercept provides the coupling efficiency η.
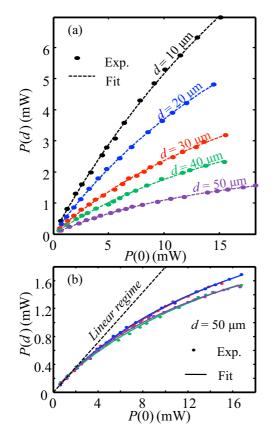
FIG. 4. (Color online) Experimental evidence of nonlinear absorption. (a) Average output power $P(d)$ carried by the SPP as a function of input power $P(0)$ for varying waveguide lengths d. Dots are experimental data and dashed lines are fits using Eq. (9). β_{eff} is the fit parameter. (b) $P(d)$ vs $P(0)$ for four waveguides with $d = 50\,\mu\mathrm{m}$. Dots are experimental data, solid lines represent fits, and the dashed line is the output power dependency in the linear regime: $P(0)e^{-\alpha_{\mathrm{eff}}d}$.

increased, and verifying that dispersion plays a weak role for 100 fs pulses [24], we measure the average output power as a function of the average input power for several waveguides. Figure 4 shows $P(d)$, the average power carried by the SPP after propagating over a distance d, as a function of $P(0)$, the average power carried by the SPP at the input of the waveguide. The graph in panel (a) compares waveguides with varying lengths d, while the graphs in panel (b) show the data obtained for four waveguides with $d = 50\,\mu\mathrm{m}$. All devices show a clear deviation from the linear regime as the power is increased. For the case of Fig. 4(a), we see that this deviation increases when d is increased, thus indicating that the coupler and decoupler are weakly nonlinear and that the nonlinear propagation is the major contributor to the observed self-action. These observations are expected from the saturable behavior suggested by Eq. (9). Since the relation between the average power P and the peak power density S of the SPP is $P = S\tau\nu_{\mathrm{rep}}\pi^{1/2}\phi_L/2$, where ϕ_L is the beam width, we are able to fit each experimental curve from Fig. 4 with Eq. (9). The only fit parameter is β_{eff}. The ensemble-averaged nonlinear absorption coefficient obtained from the fitting is $\langle\beta_{\mathrm{eff}}\rangle = (0.15 \pm 0.03)\,\mathrm{kW}^{-1}$. This nonlinear absorption coefficient is large and is comparable to the effective nonlinear

absorption coefficient of slow-light Si photonic-crystal waveguides etched in a 220 nm membrane exhibiting a slowdown factor of 10, which are known to support large two-photon absorption ($\beta_{\mathrm{PCW}} \sim 0.2\,\mathrm{kW}^{-1}$) [27].

To assert that the self-action measured is indeed ultrafast, i.e., induced and measured by a single pulse, and is not probed on average by many pulses, which would result in a nonlinearity that is dependent on the average power of the laser, we perform an additional experiment in which we consider two repetition rates ν_{rep} of the incoming laser and characterize three 50-$\mu\mathrm{m}$-long waveguides. Using a pulse picker (Pockell's cell) we are able to reduce ν_{rep} by a factor of 10 and compare the renormalized output power P_{out} as a function of the input pulse energy for two situations ($\nu_{\mathrm{rep}} = 80\,\mathrm{MHz}$ as red dots on Fig. 5,
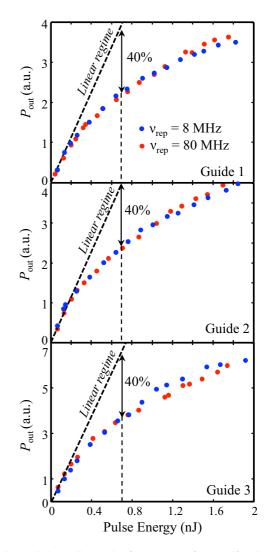

FIG. 5. (Color online) Ultrafast nature of the self-action. Raw renormalized output power P_{out} measured on the experimental setup as a function of the pulse energy for three different $50\,\mu\mathrm{m}$ waveguides and for two different repetition rates: $\nu_{\mathrm{rep}} = 8\,\mathrm{MHz}$ (blue dots) and $\nu_{\mathrm{rep}} = 80\,\mathrm{MHz}$ (red dots) of the laser. The dashed line is the linear evolution of the output power as a function of the pulse energy and is valid only at small pulse energies. The double-sided arrow indicates the position where a 40% deviation from the linear regime is observed and defines a threshold nonlinear pulse energy. All guides present almost identical threshold energies for both repetition rates.

which is the native repetition rate of the laser and $\nu_{\text{rep}} = 8$ MHz as blue dots in Fig. 5, which is the repetition rate of the laser after going through the picker). We see that the deviation from the linear regime observed is identical for both repetition rates. We have placed a 40% deviation from linearity mark on each graph, which we use to define a threshold energy. As can been seen, all waveguides present almost identical thresholds for both repetition rates. This is a clear indication that the nonlinearity is produced and probed by single pulses, i.e., on the order of a 100 fs and is therefore ultrafast.

IV. NUMERICAL SIMULATIONS AND DISCUSSION ON THE THIRD-ORDER NONLINEAR SUSCEPTIBLITY OF GOLD

Prior to retrieving Im$\{\chi^{(3)}\}$, we apply a correction to Im$\{\varepsilon_{\text{m}}\}$ using the measured α_{eff} and Re$\{\varepsilon_{\text{m}}\}$ given by [28]. We make this correction because the exact dielectric constant of our gold substrate is not known. By considering that defects in the gold surface are likely to affect Im$\{n_{\text{eff}}\}$ more than Re$\{n_{\text{eff}}\} \sim 1$, we factor out $[\text{Re}\{\varepsilon_{\text{m}}\}/(1 + \text{Re}\{\varepsilon_{\text{m}}\})]^{1/2}$ in the expression of n_{eff} and do a first-order Taylor expansion, which produces the correction Im$\{\varepsilon_{\text{m}}\} \sim \alpha_{\text{eff}}\lambda \,\text{Re}\{\varepsilon_{\text{m}}\}^2/(2p) = 2.4$. With this correction, we find Im$\{\chi^{(3)}\} \sim 3 \times 10^{-16}\,\text{m}^2/\text{V}^2$. This value is three orders of magnitude larger than the $\chi^{(3)}$ value given in [29]. Though we are unable to explain this discrepancy, we provide a discussion on the possible reasons for disagreement in [24]. However, our value is closer to the $\chi^{(3)}$ originating from interband contributions given by Hache *et al.* [15], and simulations detailed in [24] using the formalism from [30] show that it is consistent within one order of magnitude with the experiment performed in [31].

To ensure that both our model and our experiment are accurate, we simulate the nonlinear propagation of the SPP on an air/gold interface, where the gold exhibits an Im$\{\chi^{(3)}\}$ equal to our measured value. For the simulation, we use the method described in [21] and compute $P(d)$ as a function of $P(0)$. Figure 6 compares the calculated $1/P(d)$ vs $P(0)$ (dots) with the experimental fits of the same quantity for $d = 10$, 20, 30, 40, and 50 μm (solid lines). We see that the numerical simulations agree well with our experiment, further supporting our model and the retrieved Im$\{\chi^{(3)}\}$.

It should be noted that the underlying mechanism behind this nonlinear absorption could possibly be due to *direct* two-photon absorption, in which case Im$\{\chi^{(3)}\}$ is proportional to the two-photon absorption coefficient of gold. By *direct*, we mean that the two-photons are absorbed simultaneously. However, in the case where this nonlinear absorption is due to a modification of the dielectric constant of gold due to excess free carriers generated by interband absorption [15], Im$\{\chi^{(3)}\}$ is actually related to the generation of a carrier through a single-photon absorption process and a subsequent modification of the absorption properties of gold. This results in an effective two-photon absorption, but involves two different time constants instead of one, as the excess carrier generated has a lifetime that is not related to its generation by single-photon absorption. Though the contribution of interband absorption to ε_{m} is weaker than the contribution of free-electron collisions described by the Drude model
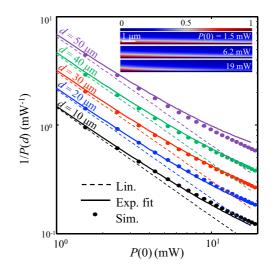

FIG. 6. (Color online) Numerical evidence of nonlinear absorption using the retrieved Im$\{\chi^{(3)}\}$. (a) $1/P(d)$ vs $P(0)$. Solid lines are linear fits to the experimental data and dots are numerical points. This representation illustrates the varying deviation from linearity for several waveguide lengths d. The inset shows the longitudinal component of the time-averaged Poynting vector shown over a 10 μm length for several average input powers. Each color plot is normalized to its maximum value.

at $\lambda = 800$ nm, it is still present. In 1988, Hache *et al.* [15] theoretically discussed a variety of mechanisms that contribute to the optical Kerr effect in metal particles, and more specifically in gold particles. Among the major contributors to the effective nonlinear susceptibility that are independent of the nanoparticle size is the interband contribution. The interband transition corresponds to carriers transitioning from the upper d-valence band to the sp-conduction bands. They argue that the dielectric constant of the metal that is due to interband transitions $\varepsilon_{\text{inter}}$ can be obtained experimentally by subtracting the dielectric constant given by the Drude model ε_{D} from the total experimental dielectric constant of the metal ε_{m} [28]. So the absorbed power density due to the interband transition can be estimated by

$$\wp \sim \frac{1}{2Z_0}\text{Im}\{\varepsilon_{\text{m}} - \varepsilon_{\text{D}}\}\,k_0|E|^2, \tag{14}$$

where Z_0 is the impedance of free-space. This equation informs on the amount of power that is absorbed to generate excess free carriers. The absorption of a photon that produces such an interband transition will generate excess free carriers per unit volume N_{ex}. These excess carriers modify the imaginary part of the dielectric constant of gold by

$$\delta\,\text{Im}\varepsilon = N_{\text{ex}}\frac{\partial\,\text{Im}\varepsilon}{\partial N} \sim \frac{\wp\tau}{\hbar\omega}\frac{\partial\,\text{Im}\varepsilon}{\partial N}, \tag{15}$$

where $\partial\,\text{Im}\varepsilon/\partial N$ is the modification of the imaginary part of the dielectric constant per unit free-carrier concentration. Here we have made the assumption that the carrier lifetime is much larger than the pulse duration τ, such that we may consider the effective absorbed energy that contributes to the modification of the dielectric constant to be equal to $\sim\wp\tau$. In our opinion, it is reasonable to make this assumption as recent experiments made at the same wavelength as our laser

in gold nanoparticles reveal that light undergoes a long two-step two-photon absorption process [18]. In this process, a first photon is absorbed to produce an interband transition from the valence to the conduction band, thus leaving a hole in the upper level of the d band. Then a second photon is absorbed producing a transition from a lower to the upper level of the d band. In this experiment, it was demonstrated that the time interval separating two consecutive absorptions is about 4 ps. This observation suggests that a free-carrier generated in the conduction band has a long lifetime consistently with our assumption. It should be noticed that the work reported in [18] is carried out using a 60-fs laser at $\lambda = 800$ nm, i.e., using a similar laser source to ours. Though the experiment is done using 50-nm gold nanoparticles, which is different to a gold film, we do not expect this process to be highly dependent on the geometry and the size of the system.

Since N_{ex} is much smaller than the total amount of free carriers in gold (N_0), we can write that

$$\frac{\partial \, \mathrm{Im}\varepsilon}{\partial N} \sim \frac{1}{N_0 \rho \varepsilon_0 \omega}, \tag{16}$$

where ρ is the resistivity of gold. Substituting $\partial \, \mathrm{Im}\varepsilon / \partial N$ and $\wp$ with their expressions in the formula for $\delta \, \mathrm{Im}\varepsilon$, we may proceed to identify it with the form

$$\delta \, \mathrm{Im}\varepsilon \sim \tfrac{3}{4} \mathrm{Im}\{\chi^{(3)}\} |E|^2, \tag{17}$$

where $\chi^{(3)}$ is the effective nonlinear susceptibility due to the effect of these excess carriers. This enables us to derive the following relation:

$$\mathrm{Im}\{\chi^{(3)}\} = \frac{2}{3} \frac{\tau}{\hbar \omega} \frac{\mathrm{Im}\{\varepsilon_m - \varepsilon_D\}}{N_0 \rho}. \tag{18}$$

To evaluate this formula numerically, we use $\rho = 22.14 \, \mathrm{n\Omega \, m}$ and $N_0 = 5.9 \times 10^{22} \, \mathrm{cm}^{-3}$ [32]. $\varepsilon_D = 1 - \omega_p^2 / [\omega(\omega + i\gamma)]$ is the dielectric constant of gold given by the Drude model with $\omega_p = 2\pi \times 2069 \, \mathrm{THz}$ and $\gamma = 2\pi \times 17.65 \, \mathrm{THz}$ [28]. Using this relation, we find

$\mathrm{Im}\{\chi^{(3)}\} \sim 2 \times 10^{-16} \, \mathrm{m^2/V^2}$. This value is very close to our experimental value and suggests that these excess carriers could indeed be responsible for the large nonlinear response. However, carrier recombination times shorter than the pulse duration will reduce the effective nonlinear response. We expect the recombination time to be highly dependent on the quality of the gold surface (roughness) and the geometry of the plasmonic interface (semi-infinite film, finite film, metal/insulator/metal, V groove, and cylindrical wires).

V. CONCLUSION

We have developed a formalism that describes self-action of SPPs at single air/metal interfaces which enables us to predict how the power carried by the SPP evolves as it propagates in the nonlinear regime. We test this relation experimentally and measure large self-action of SPPs on an air/gold waveguide. Our model, simulations, and experiment all indicate a very large imaginary third-order nonlinear susceptibility. The results presented here have important implications for the study and design of nonlinear plasmonic systems and metamaterials as the strong nonlinear absorption will compete with other desirable nonlinear optical phenomena such as third-harmonic generation or four-wave mixing [33–35], however, it also provides a mechanism to achieve ultrafast plasmonic modulation.

[1] H. Raether, *Surface Plasmons on Smooth and Rough Surfaces and on Gratings* (Springer, New York, 1998).

[2] M. Kauranen, and A. V. Zayats, Nonlinear plasmonics, Nat. Photonics **6**, 737 (2012).

[3] K. F. MacDonald, Z. L. Samson, M. I. Stockman, and N. I. Zheludev, Ultrafast active plasmonics, Nat. Photonics **3**, 55 (2009).

[4] N. I. Zheludev, The road ahead for metamaterials, Science **328**, 582 (2010).

[5] Y. Liu, G. Bartal, D. A. Genov, and X. Zhang, Subwavelength discrete solitons in nonlinear metamaterials, Phys. Rev. Lett. **99**, 153901 (2007).

[6] H. Suchowski, K. O'Brien, Z. J. Wong, A. Salandrino, X. Yin, and X. Zhang, Phase-mismatch-free nonlinear propagation in optical zero-index materials, Science **342**, 1223 (2013).

[7] E. Feigenbaum and M. Orenstein, Plasmon-soliton, Opt. Lett. **32**, 674 (2007).

[8] A. R. Davoyan, I. V. Shadrivov, A. A. Zharov, D. K. Gramotnev, and Y. S. Kivshar, Nonlinear nanofocusing in tapered plasmonic waveguides, Phys Rev. Lett. **105**, 116804 (2010).

[9] A. Degiron and D. R. Smith, Nonlinear long-range plsamonic waveguides, Phys. Rev. A **82**, 033812 (2010).

[10] C. Argyropoulos, C. Ciraci, and D. R. Smith, Enhanced optical bistability with film-coupled plasmonic nanocubes, Appl. Phys. Lett. **104**, 063108 (2014).

[11] H. Aouani, M. Rahmani, M. Navarro-Cia, and S. A. Maier, Third-harmonic-upconversion enhancement from a single semiconductor nanoparticle coupled to a plasmonic antenna, Nat. Nanotech. **9**, 290 (2014).

[12] W. Cai, A. P. Vasudev, and M. L. Brongersma, Electrically controlled nonlinear generation of light with plasmonics, Science **333**, 1720 (2011).

[13] I. De Leon, J. E. Sipe, and R. W. Boyd, Self-phase modulation of surface plasmon polaritons, Phys. Rev. A **89**, 013855 (2014).

[14] A. Marini, M. Conforti, G. Della Valle, H. W. Lee, Tr. X. Tran, W. Chang, M. A. Schmidt, S. Longhi, P. St. J. Russel, and F. Biancalana, Ultrafast nonlinear dynamics of surface plasmon polaritons in gold nanowires due to the intrinsic nonlinearity of metals, New J. Phys. **15**, 013033 (2013).

[15] F. Hache, D. Ricard, C. Flytzanis, and U. Kreibig, The optical Kerr effect in small metal particles and metal colloids: The case of gold, Appl. Phys. A **47**, 347 (1988).

[16] R. W. Boyd, Z. Shi, and I. De Leon, The third-order nonlinear optical susceptibility of gold, Opt. Commun. **326**, 74 (2014).

[17] R. W. Boyd, *Nonlinear Optics*, 3rd ed. (Academic, New York, 2008).

[18] X.-F. Jiang, Y. Pan, C. Jiang, T. Zhao, P. Yuan, T. Venkatesan, and Q.-H. Xu, Excitation nature of two-photon photoluminescence of gold nanorods and coupled gold nanoparticles studied by two-pulse emission modulation spectroscopy, J. Phys. Chem. Lett. **4**, 1634 (2013).

[19] O. Lozan, M. Perrin, B. Ea-Kim, J. M. Rampnoux, S. Dilhaire, and P. Lalanne, Anomalous light absorption around subwavelength apertures in metal films, Phys. Rev. Lett. **112**, 193903 (2014).

[20] G. P. Agrawal, *Nonlinear Fiber Optics*, 4th ed. (Academic, New York, 2007), Chap. 2.

[21] A. Baron, S. Larouche, D. J. Gauthier, and D. R. Smith, Scaling of the nonlinear response of the surface plasmon polariton at a metal/dielectric interface, J. Opt. Soc. Am. B **32**, 9 (2015).

[22] Q. Lin, J. Painter, and G. P. Agrawal, Nonlinear optical phenomena in silicon waveguides: Modeling and applications, Opt. Express **15**, 16604 (2007).

[23] L. Yin and G. P. Agrawal, Impact of two-photon absorption on self-phase modulation in silicon waveguides, Opt. Lett. **32**, 2031 (2007).

[24] See Supplemental Material at http://link.aps.org/supplemental/10.1103/PhysRevB.91.195412 for a comprehensive derivation of the theoretical model and additional information on the experimental setup used for the measurements. Comparison are also made between our measured third-order nonlinear susceptibility of gold and past values given in literature.

[25] P. Lalanne, J. P. Hugonin, H. T. Liu, and B. Wang, A microscopic view of the electromagnetic properties of sub-λ metallic surfaces, Surf. Sci. Rep. **64**, 453 (2009).

[26] A. Baron, E. Devaux, J.-C. Rodier, J.-P. Hugonin, E. Rousseau, C. Genet, T. W. Ebbesen, and P. Lalanne, Compact antenna for efficient and unidirectional launching and decoupling of surface plasmons, Nano. Lett. **11**, 4207 (2011).

[27] C. Monat, B. Corcoran, M. Ebnali-Heidari, C. Grillet, B. J. Eggleton, T. P. White, L. O'Faolain, and T. F. Krauss, Slow light enhancement of nonlinear effects in silicon engineered photonic crystal waveguides, Opt. Express **17**, 2944 (2009).

[28] P. B. Johnson and R. W. Christy, Optical constants of the noble metals, Phys. Rev. B **6**, 4370 (1972).

[29] I. De Leon, Z. Shi, A. C. Liapis, and R. W. Boyd, Measurement of the complex nonlinear optical response of a surface plasmon-polariton, Opt. Lett. **39**, 2274 (2014).

[30] R. R. Alfano, P. L. Baldeck, P. P. Ho, and G. P. Agrawal, Cross-phase modulation and induced focusing due to optical nonlinearities in optical fibers and bulk materials, J. Opt. Soc. Am. B **6**, 824 (1989).

[31] N. Rotenberg, A. D. Bristow, M. Pfeiffer, M. Betz, and H. M. van Driel, Nonlinear absorption in Au films: Role of thermal effects, Phys. Rev. B **75**, 155426 (2007).

[32] J. Babiskin and J. R. Anderson, *American Institute of Physics Handbook* (McGraw-Hill, New Yotk, 1972), pp. 9–39.

[33] M. Lippitz, M. A. van Dijk, and M. Orrit, Third-harmonic generation from single gold nanoparticles, Nano. Lett. **5**, 799 (2005).

[34] S. Palomba and L. Novotny, Nonlinear Excitation of surface-plasmon polaritons by four-wave mixing, Phys. Rev. Lett. **101**, 056802 (2008).

[35] J. Renger, R. Quidant, N. van Hulst, and L. Novotny, Surface-enhanced nonlinear four-wave mixing, Phys. Rev. Lett. **104**, 046803 (2010).